European Journal of Medical Research

RESEARCH

Open Access

Diagnostic and prognostic significance of tetraspanin 6 and its role in facilitating glioma progression

Longqi Sa[1,2†], Junwei Jiang[2†], Yifan Li[3†], Yi Huo[2], Wenjing Zheng[2], Han Zhang[1,2], Lingling Zhang[2], Tao Wang[2*] and Lequn Shan[1*]

Abstract

Background Several tetraspanin (TSPAN) proteins have been implicated in tumorigenesis and disease progression. However, the precise function of tetraspanin 6 (TSPAN6) in glioma remains unclear.

Methods Integrated raw data from the Tumor Genome Atlas (TCGA) and Gene Expression Profiling (GEO) databases were processed using R4.2.1. Bioinformatic methods were used to analyze the gene expression levels of TSPAN6 in both glioma and normal brain tissues, correlating them with clinical characteristics. Additionally, the predictive value of TSPAN6 in relation to the immune checkpoint blockade (ICB) therapy response was assessed. In vitro experiments were conducted to investigate the effects of TSPAN6 knockdown on glioma cell proliferation, migration, cell cycle regulation, and macrophage recruitment.

Results TSPAN6 expression was significantly upregulated in glioma tissues compared to normal tissues. Elevated TSPAN6 expression is strongly correlated with unfavorable clinical characteristics in gliomas. Bioinformatic analyses revealed a significant correlation between elevated TSPAN6 expression and reduced overall survival. Additionally, TSPAN6 was co-expressed with several immune checkpoint genes and revealed a prognostic value in the context of ICB therapy. Functional enrichment analysis revealed the involvement of TSPAN6 in cell-cycle regulation. Furthermore, TSPAN6 expression positively correlated with macrophage and neutrophil infiltration. In vitro experiments confirmed that the downregulation of TSPAN6 inhibited U251 cell proliferation, disrupted the cell cycle, diminished migratory capabilities, and reduced the recruitment of macrophages.

Conclusion Our findings emphasize its potential as both a diagnostic and therapeutic target as well as a predictor of immune therapy response in gliomas.

Keywords Glioma, TSPAN6, Prognosis, Immune infiltration, Immune checkpoint

†Longqi Sa, Junwei Jiang and Yifan Li have equally contributed to this work.

*Correspondence:
Tao Wang
wangt@fmmu.edu.cn
Lequn Shan
drshanlq@fmmu.edu.cn
Full list of author information is available at the end of the article

Introduction

Gliomas are a type of tumor derived from glial cells and neural precursor cells, and they are the most frequently occurring primary malignant tumors of the brain or spinal cord. It primarily has astrocytic, oligodendroglial, and ependymal cell origins. Despite the use of various treatment regimens in clinical practice, the high fatality rate of patients remains primarily due to the specificity of tumor site location [1]. Over several decades, significant progress has been made in understanding the molecular basis of tumors thanks to the continuous development of genomics, epigenetics, and transcriptomic analyses. This has provided new insights into the improvement of tumor classification and molecular-targeted therapies. In 2016, the World Health Organization incorporated certain molecular pathological features into the diagnostic system for gliomas [2], and in 2021, the importance of these features was further emphasized. For example, specific molecular pathological features, such as IDH mutations, 1p/19q co-deletions, and MGMT gene promoter methylation, have been more accurately used in the grading and classification of gliomas [3]. Therefore, exploration of new therapeutic targets and prognostic biomarkers to guide clinical treatment is of great significance.

The tetraspanin (TSPAN) protein family consists of intracellular loops, transmembrane domains, and extracellular loops [4, 5]. These proteins primarily reside on the cell membrane and are characterized by four hydrophobic structural domains. The TSPAN protein family plays crucial physiological roles in cell development, activation, growth, and movement regulation. The expression of TSPAN1 has been identified as an unfavorable prognostic factor in patients with stage II and III gastric cancer [6]. Moreover, TSPAN1 promotes migration and invasion of pancreatic cancer cell lines via phospholipase Cγ (PLCγ) [7]. Furthermore, TSPAN8 inhibits the proliferation and migration of breast cancer cell lines by suppressing their nuclear translocation [8]. TSPAN6 inhibits tumor development in both lung and breast cancers [9, 10]. In addition, the TSPAN protein family is involved in the modulation of the immune system and inflammation. Notably, TSPAN26 is involved in immune regulation and tumor suppression as a surface antigen in mature B cells [11]. However, the precise role of TSPAN6 in glioma development has not been investigated thoroughly.

The tumor microenvironment (TME) plays a promoting role in the development of most tumors. Tumor-associated macrophages (TAMs), including glioma-specific microglia, are the predominant immune cells in the glioma TME. These two types of macrophages have been found to be positively correlated with glioma grade, frequently leading to unfavorable prognosis in patients with glioma [12]. Further research has revealed that neutrophils in gliomas promote tumor growth and infiltration and are associated with acquired resistance to anti-angiogenic therapy [13, 14]. Additionally, immune cells in the TME express multiple immune checkpoint molecules that, when activated, inhibit the function of immune cells and contribute to tumor development. Therefore, blocking of these inhibitory immune checkpoints is an effective therapeutic strategy. Presently, specific inhibitory immune checkpoint inhibitors, including anti-cytotoxic T-lymphocyte-associated protein 4 (anti-CTLA4) [15] and anti-programmed cell death 1 (anti-PD-1) [16], have been utilized in clinical settings for various cancers and have demonstrated promising efficacy. However, immune checkpoint blockade has not yielded the expected results in treating glioma owing to the unexplained underlying mechanisms [17]. Therefore, the identification of molecules that can predict the efficacy of immune checkpoint blockade is crucial for choosing immunotherapy strategies for gliomas.

In this study, we identified aberrant expression of TSPAN6 in gliomas using data from The Cancer Genome Atlas (TCGA) and Gene Expression Overview (GEO) databases. Bioinformatic analyses revealed that high TSPAN6 expression was associated with unfavorable clinical characteristics and patient outcomes. Notably, the expression of TSPAN6 is positively correlated with the expression of certain immune checkpoint molecules and can serve as an indicator of the effectiveness of immune checkpoint blockade. Mechanistically, TSPAN6 participates in cell cycle regulation and is closely linked to immune cell infiltration in tumors. In vitro experiments showed that the suppression of TSPAN6 hindered U251 cell proliferation, interrupted the cell cycle, diminished invasive and migratory capacities, and lowered macrophage recruitment. Overall, our study demonstrated the significance of TSPAN6 in glioma progression and suggested its potential as a diagnostic and prognostic biomarker for gliomas.

Materials and methods

Patient sample data acquiring

Patient sample data were acquired by retrieving messenger RNA (mRNA) expression data and corresponding clinical information from TCGA database (https://cancergenome.nih.gov). This dataset included 169 glioblastoma multiforme (GBM) samples, 532 lower-grade glioma (LGG) samples, and 5 neighboring brain tissue samples. Data regarding gene expression in normal brain tissue were obtained from the GTEx database (https://www.gtexportal.org). Furthermore, the gene expression profile GSE4290 was downloaded from the GEO database (https://www.ncbi.nlm.nih.gov/geo/) and contained 23 samples from neighboring brain tissues and 153 samples

of gliomas. Protein expression data for 99 GBM samples and 10 normal brain tissue samples were acquired from the UALCAN database (http://ualcan.path.uab.edu/). These databases contain data on the mRNA and protein expression of prevalent tumors.

Patient survival analysis

Kaplan–Meier (KM) analysis of glioma patients in TCGA dataset was conducted using the R software packages Survival (versions/3.3.1) and Survminer to investigate the impact of TSPAN6 expression on overall survival time (OS), disease-specific survival (DSS), and progression-free survival (PFS). To determine whether TSPAN6 expression can distinguish tumor tissue from normal tissue samples, the package proc (https://crean.rproject.org/web/Packages/proc/) to generate receiver operating characteristic (ROC) curves was used.

Genetic mutation analysis

The mutation status of TSPAN6 was determined using cBioPortal for Cancer Genomics [18, 19]. To further explore the mutation types of TSPAN6 in gliomas, the COSMIC database was used [20].

Functional enrichment analysis

A threshold of 350 for TSPAN6 mRNA expression was used to divide the 699 patients with glioma into two groups: high expression ($n=350$) and low expression ($n=349$). The LIMMA software package in R (version 4.2.1) was employed to identify differentially expressed genes (DEGs) between the high- and low-expression groups of TSPAN6. DEGs were identified using the criteria of adjusted p-value <0.05 and |log fold change| (|logFC|) ≥ 1. Subsequently, KEGG and GO enrichment analyses were performed using the screened DEGs to investigate the potential involvement of TSPAN6 in gliomas. Gene set enrichment analysis (GSEA), a method for determining differences in the expression of a predefined group of genes across multiple samples, was conducted using the R package ClusterProfiler to examine functional and pathway differences between the high and low-expression groups of TSPAN6 in gliomas [21]. The significant enrichment criteria were set at an adjusted p-value <0.05, a false discovery rate (FDR) <0.25, and |NES| >1.

Hub gene screening

To identify hub genes, we constructed a protein–protein interaction (PPI) network using the STRING database (http://string-db.org) with an interaction score greater than 0.4. Subsequently, the network data were imported into the Cytoscape program (version 3.9.1) and the nodes were ranked based on their degrees using the cytoHubba plugin. Finally, GO and KEGG analyses were performed to investigate the functions and pathways associated with the identified hub genes.

Examination of immune infiltration

To assess the level of immune cell infiltration in the glioma microenvironment, single-sample gene set enrichment analysis (ssGSEA) was performed on the TSPAN6 high-expression and low-expression groups using the R package GSVA (Version 4.2.1). A set of 24 immune cell gene markers, identified in a previous study [22], was used. Spearman's correlation test was used to evaluate the association between TSPAN6 and the aforementioned 24 immune cell types.

Predicting the value of TSPAN6 in immune checkpoint blockade therapy response

Tumor Immune Dysfunction and Exclusion (TIDE), a computational system, was utilized to analyze the potential for tumor immune evasion and to predict the effectiveness of immune checkpoint blockade therapy based on the gene expression profiles of tumor samples. To assess TSPAN6's response to immune checkpoint blockade (ICB), this approach was employed [23, 24]. Additionally, the IMvigor210 cohort treated with anti-PDL1 therapy was downloaded to further validate the previous response of TSPAN6 to immune checkpoint blockade [25].

Cell culture, vector construction and lentivirus packaging

293T embryonic kidney, THP-1 mononuclear leukemia, and U251 glioma cell lines were obtained from Procell Life Science & Technology Co., Ltd., Wuhan, China. THP-1 cells were cultured in RPMI-1640, whereas U251 and 293T cells were cultured in DMEM. All cell lines were supplemented with 10% fetal bovine serum (Gibco). The cells were then incubated at 37 °C with 5% CO_2. The shTSPAN6 sequence was inserted into the hU6-MCS-Ubiquitin-EGFP-IRES-puromycin lentivirus vector (provided by Shanghai Genechem Co., Ltd.), which contained puromycin resistance and green fluorescent protein (GFP). HEK293T cells were transfected with the plasmid along with PMD2G and psPAX2 vectors using a three-plasmid system. After 48 h of culture, the viral supernatants were collected. U251 cells were infected with the viral supernatant for 12 h and then cultured in a medium supplemented with puromycin for 1 week to select stably transfected cell lines. The sequences of the three shRNA constructs were as follows: shTSPAN6-1,5′-gctactggtaccgtcattatt-3′; shTSPAN6-2,5′-cctaagagttgctgtaaactt-3′; shTSPAN6-3,5′-gcttccaactgattggaatct-3′.

Quantitative real-time fluorescent quantification PCR (qRT-PCR) assay

RNA extraction from stably transfected cell lines and cell lines from the control group was performed using a MiniBEST reagent kit (TaKaRa, Shiga, Japan). qRT-PCR analysis was conducted using TB Green Premix Ex TaqTM II (Takara, Shiga, Japan), and the calculation was based on the 2-CT method. Complementary deoxyribonucleic acid (cDNA) was synthesized using the PrimerScript RT Reagent Kit (TaKaRa, Shiga, Japan). The forward and reverse primer sequences for TSPAN6 were 5′-TCGGAG ACTGCAGACTAAACC-3′ and 5′-ACGCCAGTGATC CAGAAAAT-3′, respectively. The forward and reverse primer sequences for β-actin were 5′-GACAGCTCT CCCAGGAAT-3′ and 5′-CTCCTTAATGTCACGCAC GAT-3′, respectively.

Western blot (WB) assay

WB assay was performed to validate the changes in TSPAN6 protein levels. U251 cells were lysed using radioimmunoprecipitation assay (RIPA) lysis buffer to extract total protein, and the protein concentration was quantified using a BCA reagent kit (Solarbio, China). Subsequently, 10 μg of protein was separated using PAGE (Mishushengwu, China) and transferred onto a polyvinylidene fluoride (PVDF) membrane. After blocking with 5% skimmed milk for 1 h, the membrane was incubated overnight at 4 °C with specific antibodies against TSPAN6 and β-actin (Proteintech). On the following day, the membrane was washed with TBST (25 mM Tris–HCl, 150 mM NaCl, 0.05% Tween 20, and a pH of 7.4) for 30 min, incubated with secondary antibodies (Proteintech, China) at room temperature for 1 h, washed again with TBST for 30 min, and finally observed using an enhanced chemiluminescence (ECL) reagent kit.

Cell proliferation analysis

U251 cells were seeded in a 96-well plate at a density of 4×10^3 cells per well 24 h before use. 10 mg of CCK-8 reagent were added at 24, 48, 72, and 96 h. The cells were incubated for an additional hour at 37 °C and 5% CO_2. The absorbance was measured using an enzyme-linked immunosorbent assay reader at a wavelength of 450 nm.

Cell scratch assay

U251 cells were seeded at a density of 3×10^5 cells per well in a 6-well plate. Once the cells had reached over 90% confluence, three PBS washes were performed, followed by vertical scraping of the cells using a 20 μL sterile pipette tip. Subsequently, the cells were cultured in DMEM without serum for a full day. The wound-healing state was monitored, and photographs were taken at 0 and 24 h. ImageJ software was used to process the images.

Transwell assay

U251 cells were starved in a serum-free environment for 24 h, harvested, and centrifuged. The cells were resuspended in DMEM without serum, and the cell density was adjusted to 1×10^4 cells/mL. Next, 200 μL of the cell suspension was added to Transwell chambers filled with a matrix gel. The lower chamber was filled with 600 μL of culture medium containing 10% FBS. The chambers were incubated at 37 °C with 5% CO_2 for 48 h. Subsequently, the chambers were removed and the upper surface of the membranes was gently swabbed using a cotton swab to remove the cells. The cells on the bottom surface were fixed in 95% ethanol for five minutes and stained with a 0.4% crystal violet solution for 20 min. After rinsing with PBS and allowing it to dry, cells were counted and examined under a microscope.

Colony formation assay

U251 cells were digested, centrifuged, and the cell density was adjusted to 1×10^3 cells/mL. Subsequently, 200 μL of the cell suspension was seeded into each well of a 6-well plate. The cells were incubated at 37 °C in a 5% CO_2 environment for 2 weeks and then rinsed twice with PBS. The cells were then fixed with 5 mL methanol for 15 min and stained with 0.4% crystal violet for 20 min. After rinsing with PBS and allowing it to dry, images were captured and the cells were counted.

Flow cytometry

Flow cytometry was used to detect the cell cycle and apoptosis. For cell cycle detection, cells in the logarithmic growth phase were collected and washed thrice with PBS. Subsequently, pre-cooled 75% ethanol at −20 °C was added to the cells, which were then incubated overnight at 4 °C. The following day, cells were washed twice with PBS and treated with a solution containing 0.01% RNase and 0.5% propidium iodide (PI) at 4 °C for 20 min. After passing through a 300-mesh nylon mesh, cells were analyzed using a flow cytometer.

For apoptosis detection, cells in the logarithmic growth phase were collected and washed once with PBS, followed by washing with the incubation buffer. The cells were then resuspended in 100 μL of incubation buffer, and 5 μL of fluorescently labeled Annexin V was added. The cells were then incubated at room temperature, protected from light, for 15 min. Subsequently, the cells were washed once with incubation buffer, resuspended, and mixed with 10 μL of 7AAD was added for mixing. Apoptotic cells were detected using flow cytometry.

Statistical analysis

For the bioinformatic study, R version 4.2.1 was used. The transcription levels of the TSPAN6 gene were compared between cancer samples and normal control samples using Student's *t*-test. The relationship between TSPAN6 expression and clinical characteristics was examined using the Kruskal–Wallis and Wilcoxon rank-sum tests. Diagnostic accuracy was assessed through ROC curve analysis, using the area under the curve (AUC) as a metric. Survival analysis was conducted using the Kaplan–Meier method, and the log-rank test was employed. Potential prognostic variables were screened using univariate and multivariate COX analyses. Spearman's correlation test was conducted to investigate the relationship between TSPAN6 expression and immune cell infiltration. In all analyses, *p*-values greater than 0.05 were denoted as ns, *p*-values less than 0.05 were denoted as *, *p*-values less than 0.01 were denoted as **, and *p*-values less than 0.001 were denoted as ***.

Results

TSPAN6 exhibited high expression in gliomas and was correlated with adverse clinical and pathological characteristics

Using data from TCGA database, we investigated the expression levels of TSPAN6 in tumor and normal tissues across various cancer types. As shown in Fig. 1a, TSPAN6 expression was significantly higher in tumor tissues of gastric cancer, endometrial cancer, lung adenocarcinoma, and esophageal cancer. Through comparative analysis, we observed that glioma tissues had markedly higher levels of TSPAN6 expression than normal tissues (Fig. 1B), consistent with the validation provided by the GSE4290 dataset (Fig. 1C). Furthermore, the UALCAN database demonstrated significantly elevated levels of TSPAN6 protein in pleomorphic glioblastoma tissues than in normal tissues (Fig. 1D). We analyzed TSPAN6 gene mutations using the cBioPortal database and found that "amplification" was predominant in TCGA pan-cancer dataset. Among the 514 LGG patients, TSPAN6 gene mutations were detected in 1.56% of the cases, including both "amplification" and "mutations" (Supplementary Figure 1).

To explore the correlation between TSPAN6 expression and clinical and gene expression features in glioma patients, we analyzed data from TCGA dataset comprising 696 glioma patients (Table 1). Based on the median TSPAN6 expression, patients were divided into two groups: high expression ($n=348$) and low expression ($n=348$). The analysis revealed a significant association between high TSPAN6 expression and adverse clinical and pathological characteristics, such as WHO grade, IDH status, histological grade, age, and 1p/19q co-deletion (Fig. 1E–I and Table 1). Therefore, the increased expression of TSPAN6 in glioma tissues correlates with negative clinical and pathological features of gliomas.

The overexpression of TSPAN6 was associated with a negative prognosis in patients with glioma

We conducted univariate and multivariate Cox regression analyses to investigate the potential association between overall survival in glioma patients and TSPAN6 expression, along with other clinical characteristics. High TSPAN6 expression was significantly correlated with patient overall survival (HR = 2.714, 95% CI = 2.103–3.502, $p<0.001$), as revealed by the results of the univariate COX analysis (Table 2). Kaplan–Meier survival analysis was used to compare the prognosis of glioma patients with high or low TSPAN6 levels. The study demonstrated that glioma patients with higher TSPAN6 expression had shorter progression-free intervals, overall survival times, and disease-specific survival times (Fig. 2A–C). Additionally, ROC analysis was performed to evaluate the diagnostic value of TSPAN6 expression in differentiating glioma from normal tissues. The results showed that TSPAN6 exhibited a reasonably high diagnostic accuracy, with an estimated AUC value of 0.987 (95% CI 0.983–0.992) (Fig. 2D). In the subgroup analysis considering WHO grade, 1p/19q non-codeletion status, astrocytoma pathological type, and primary therapy outcome, glioma patients with high TSPAN6 expression had a poor prognosis (Fig. 2E–H). To assess the impact of TSPAN6 expression on overall survival at 1, 3, and 5 years for prognostic purposes, we calculated AUC values.

The findings demonstrated that the AUC values at all three time periods exceeded 0.5 and were approximately 0.700 (Fig. 2I). We constructed a composite nomogram that incorporated TSPAN6 expression data and clinical factors to predict patient survival at 1, 3, and 5 years (Fig. 2J). Furthermore, the calibration graph exhibited strong agreement between the observed and projected values (Fig. 2K), reaffirming that TSPAN6 expression has a positive prognostic impact on glioma.

Cell cycle-associated genes and pathways were enriched in gliomas with high expression of TSPAN6

We investigated the biological functions and pathways related to TSPAN6 in gliomas using data from TCGA database. To gain insight into the biological role of TSPAN6 in gliomas, we compared the differentially expressed genes (DEGs) between the high- and low-expression groups. We identified 1555 DEGs, with 676 upregulated and 879 downregulated genes. The significance threshold for differential expression was set at $|\log2(FC)| > 1$ and $p.adj < 0.05$. The distribution of DEGs

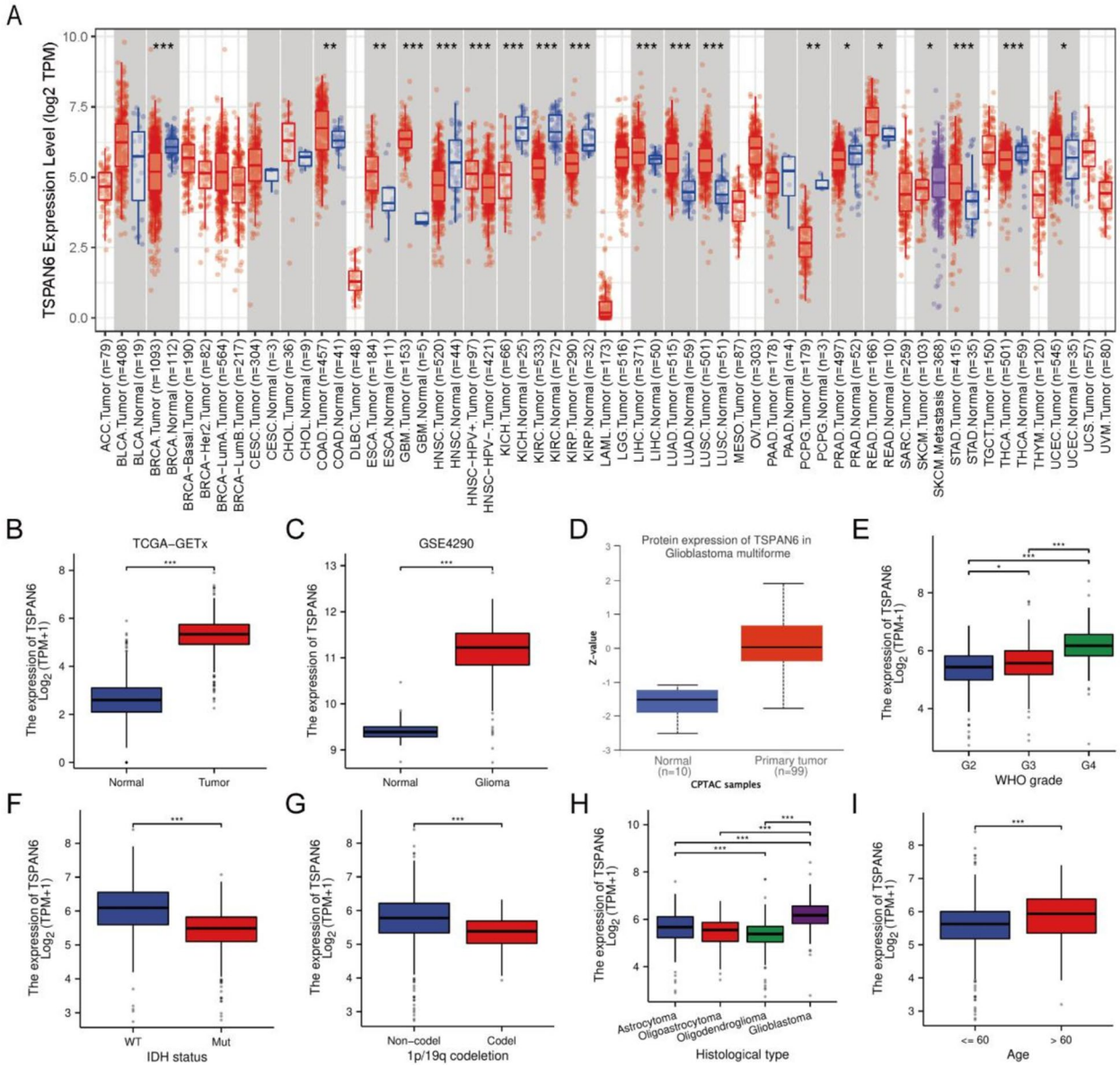

Fig. 1 Upregulation of TSPAN6 expression in glioma and its association with adverse clinical pathological features of glioma patients. **A** Expression levels of TSPAN6 in different types of human malignancies from the TIMER database. **B** Expression levels of TSPAN6 in normal tissue and tumor tissue of glioma patients. **C** Expression of TSPAN6 in tumors and normal tissues from the GEO database GSE4290 dataset. **D** Protein expression levels of TSPAN6 in GBM and normal tissues from the UALCAN database. **E**–**I** Correlation of TSPAN6 high expression with glioma clinical pathological features [WHO grade (**E**), IDH status (**F**), 1p/19q co-deletion (**G**), pathological subtype (**H**), and age (**I**)]

was visualized through heatmaps and volcano plots (Fig. 3A, B). GO and KEGG analyses of the 676 upregulated DEGs revealed significant enrichment in cell cycle signaling pathways, chromosome segregation, and mitosis (Fig. 3C, D). GSEA analysis using the MSigDB Collection identified enriched signal pathways related to TSPAN6, such as the cell cycle, DNA replication, and condensation of early mitotic chromosomes (Fig. 3E, F). These data support the possibility that TSPAN6 is involved in cell cycle signaling in gliomas.

Identification of the Hub gene in glioma tissues and its significance for prognosis in individuals with gliomas

First, DEGs from the STRING database were used to build a PPI network. Next, the hub genes were ranked according to their degrees using the cytoHubba plugin

Table 1 Clinical characteristics of patients in TCGA dataset with high or low TSPAN6 expression levels

Characteristic	Low expression of TSPAN6	High expression of TSPAN6	*p*
n	349	350	
WHO grade, *n* (%)			< 0.001
G2	146 (22.9%)	78 (12.2%)	
G3	138 (21.7%)	107 (16.8%)	
G4	30 (4.7%)	138 (21.7%)	
IDH status, *n* (%)			< 0.001
WT	68 (9.9%)	178 (25.8%)	
Mut	278 (40.3%)	165 (23.9%)	
1p/19q co-deletion, *n* (%)			< 0.001
Codel	126 (18.2%)	46 (6.6%)	
Non-codel	223 (32.2%)	297 (42.9%)	
Primary therapy outcome, *n* (%)			0.089
PD	58 (12.5%)	54 (11.6%)	
SD	90 (19.4%)	58 (12.5%)	
PR	35 (7.5%)	30 (6.5%)	
CR	93 (20%)	47 (10.1%)	
Gender, *n* (%)			0.086
Female	159 (22.8%)	139 (20%)	
Male	189 (27.2%)	209 (30%)	
Age, *n* (%)			0.012
≤ 60	291 (41.6%)	265(37.9%)	
> 60	58 (8.3%)	85 (12.2%)	
Histological type, *n* (%)			< 0.001
Astrocytoma	97 (13.9%)	99 (14.2%)	
Glioblastoma	30 (4.3%)	138 (19.7%)	
Oligoastrocytoma	145 (20.7%)	55 (7.9%)	
Oligodendroglioma	77 (11%)	58 (8.3%)	
Age, median (IQR)	41.5 (33, 54)	49 (36, 60)	< 0.001

PD progressive disease, *SD* stable disease, *PR* partial response, *CR* complete response, *IQR* interquartile range

to obtain node scores (Fig. 4A). Significant enrichment in cell cycle signaling pathways, sister chromatid separation during mitosis, and phase transition in the mitotic cell cycle was observed in the GO and KEGG analyses (Fig. 4B). TSPAN6 may be related to the cell cycle, as predicted by the biological roles and pathways of DEGs in gliomas. We then examined the relationship between TSPAN6 and the genes that control the cell cycle. The findings demonstrated a favorable correlation ($r > 0.3$, $p < 0.001$) between TSPAN6 expression and genes governing the cell cycle, such as PCNA, CCNA2, CHEK1, MCM2, CCNB2, CCNB1, CDC20, MCM6, CDC25C, PLK1, CDC6, BUB1B, PTTG1, ESPL1, CDC45, MCM4, CDC25A, and CCNE1, but a weak correlation ($r > 0.2$, $p < 0.001$) with PKMYT1 and E2F1 (Supplementary Figure 2).

The predictive significance of these 10 hub genes was determined using Kaplan–Meier survival analysis in patients with gliomas. The findings demonstrated that in the high-expression group of glioma patients, higher expression of these 10 genes was linked to worse overall survival (Fig. 4C–L). Collectively, these findings strongly indicated that TSPAN6 expression is linked to the cell cycle and may contribute to glioma progression through cell cycle regulation.

TSPAN6 promotes the cell cycle, proliferation, and migration of glioma cells

To investigate the role of TSPAN6 in glioma, stable TSPAN6-suppressed cell lines were established in U251 cells by lentiviral infection (Fig. 5A). The knockdown efficiency was confirmed by qPCR (Fig. 5B) and western blotting (Fig. 5C). Among the three TSPAN6-targeting shRNA expressing U251 cell lines, only shTSPAN6-3 exhibited significant knockdown efficiency. The growth of U251 cells was considerably reduced by TSPAN6 knockdown, as demonstrated by CCK-8 assay (Fig. 5D). Similarly, the colony-forming and proliferative capacities of cells with TSPAN6 suppression were notably decreased

Table 2 Univariate and multivariate Cox regression analyses of clinical characteristics in glioma patients in TCGA dataset were associated with overall survival (OS) correlation

Characteristics	Total (*N*)	Univariate analysis		Multivariate analysis	
		Hazard ratio (95% CI)	*P* value	Hazard ratio (95% CI)	*P* value
WHO grade (G4 vs. G2 and G3)	636	9.538 (7.243–12.560)	**< 0.001**	2.566 (1.693–3.888)	**< 0.001**
IDH status (Mut vs. WT)	688	8.609 (6.602–11.226)	**< 0.001**	4.104 (2.781–6.057)	**< 0.001**
1p/19q co-deletion (non-codel vs. codel)	691	4.435 (2.889–6.808)	**< 0.001**	1.386 (0.808–2.379)	0.236
Age (> 60 vs. ≤ 60)	698	4.696 (3.620–6.093)	**< 0.001**	1.519 (1.109–2.079)	**0.009**
Histological type (oligoastrocytoma and astrocytoma vs. oligodendroglioma and glioblastoma)	698	2.167 (1.678–2.798)	**< 0.001**	0.749 (0.475–1.180)	0.213
TSPAN6 (high vs. low)	698	2.710 (2.105–3.488)	**< 0.001**	1.191 (0.861–1.647)	0.29

The bold values indicate statistical differences

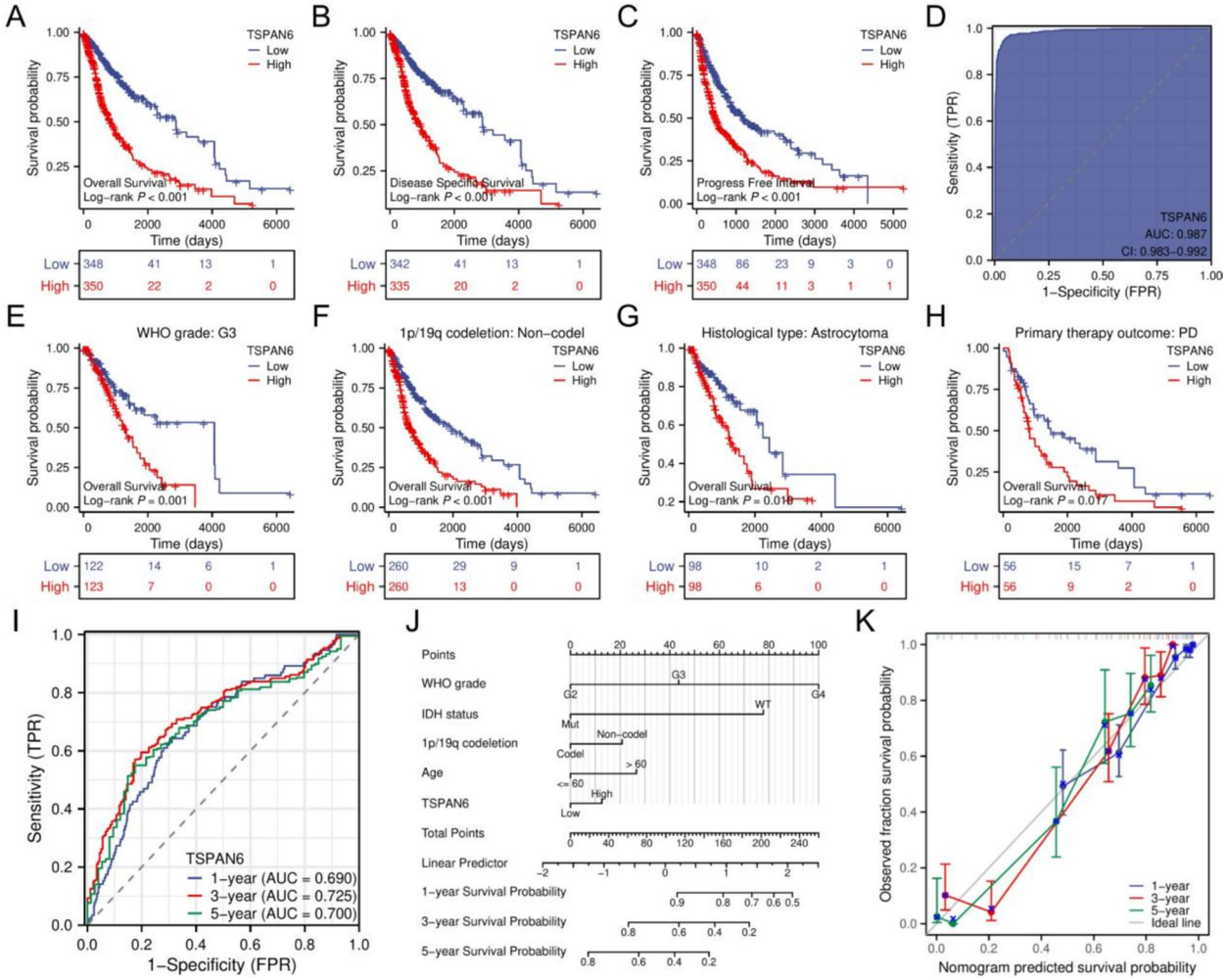

Fig. 2 Kaplan–Meier survival curves and diagnostic value analysis of TSPAN6 in glioma for prognosis. **A**–**C** Kaplan–Meier survival curves for OS, DSS, and PFI in the TCGA dataset. **D** ROC curve analysis of TSPAN6 expression in glioma and adjacent tissues. **E**–**H** Prognostic subtype analysis based on WHO grade: G3 (**E**), 1p/19q co-deletion: non-deletion (**F**), astrocytoma subtype (**G**), and disease progression (PD) (**H**). **I** AUC was calculated at 1 year, 2 years, and 5 years. **J** Nomogram survival prediction chart for predicting the 1-, 3-, and 5-year overall survival rates. **K** Calibration plot of the nomogram for OS prediction

in the colony formation assay (Fig. 5E). Flow cytometry results showed no significant difference in the apoptosis rates between the TSPAN6-suppressed and control groups (Fig. 5F). However, TSPAN6 knockdown induced obvious cell cycle arrest in the G2/M phase (Fig. 5G), consistent with previous TCGA data analysis of the role of TSPAN6 in cell cycle regulation. Finally, the scratch and transwell assays demonstrated decreased migration ability of TSPAN6 knockdown U251 cells (Fig. 5H–K). To further elucidate the role of TSPAN6 in glioma cells, we utilized the widely recognized U87 glioma cell line to overexpress TSPAN6. We successfully overexpressed TSPAN6-flag in U87 cells by using a lentiviral system (Supplementary Figure 3A). Our results indicated that TSPAN6 overexpression significantly promoted the proliferation of U87 tumor cells (Supplementary Figure 3B) and enhanced their migratory capabilities (Supplementary Figure 3C–F). Overall, these in vitro experiments suggest that TSPAN6 expression in glioma cells accelerates tumor cell cycle progression, promotes cell proliferation, and enhances migration.

TSPAN6 expression promoted infiltration of immunosuppressive immune cells and polarization of M2 macrophages in gliomas

To investigate the association between TSPAN6 expression and the tumor microenvironment (TME), we assessed the tumor purity of gliomas in groups with high

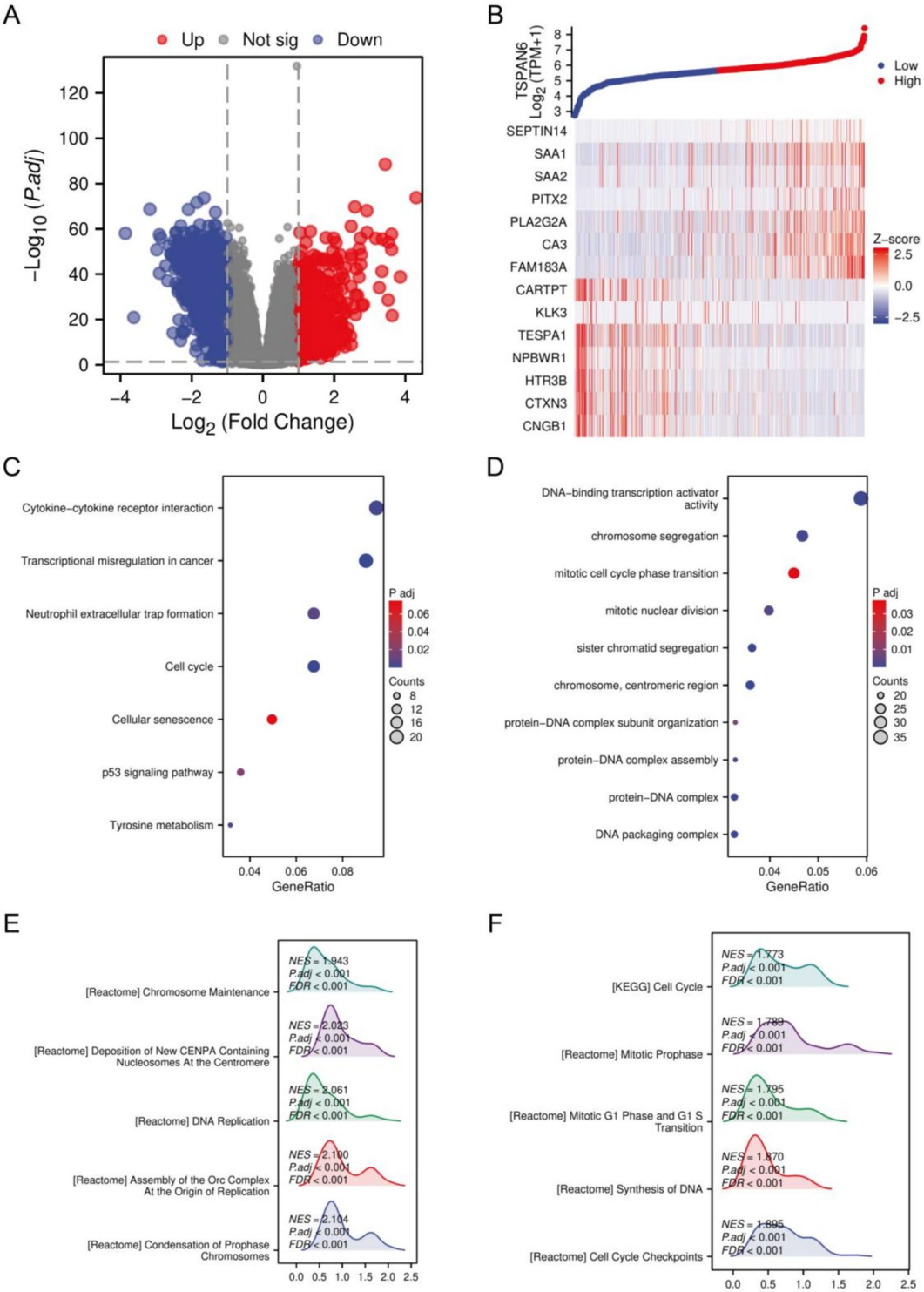

Fig. 3 Biological function and pathway prediction of TSPAN6 in glioma. **A** Volcano plot of DEGs associated with TSPAN6 expression. **B** Heatmap of the top 14 DEGs positively or negatively correlated with TSPAN6. **C**, **D** KEGG and GO enrichment analysis. **E**, **F** Enrichment landscape of GSEA. *NES* normalized enrichment score, *FDR* false discovery rate

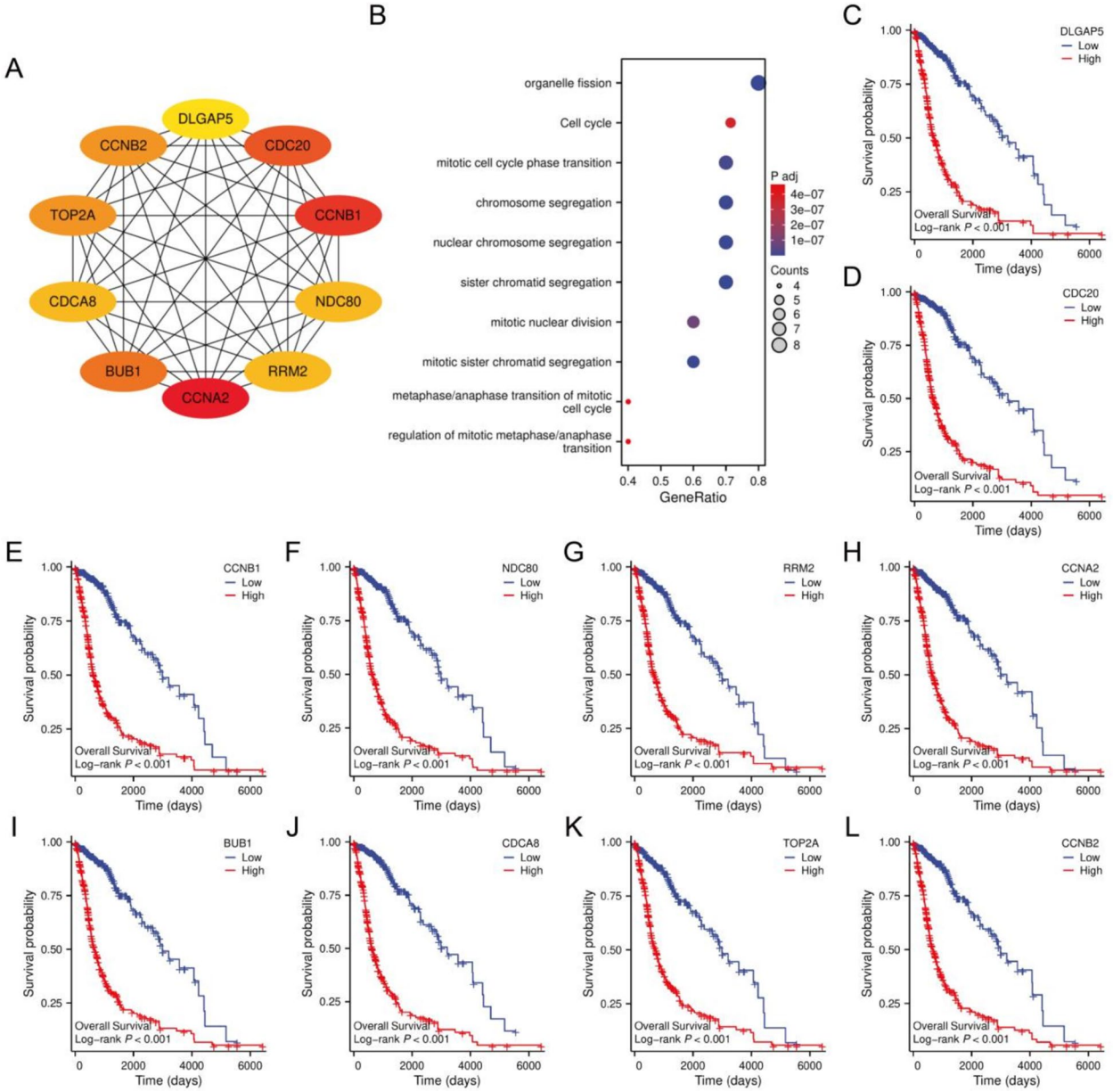

Fig. 4 Hub gene analysis. **A** Interaction network of the top ten hub genes. **B** GO and KEGG enrichment analysis of hub genes. **C**–**L** Prognostic value of ten hub genes (DLGAP5, CDC20, CCNB1, NDC80, RRM2, CCNA2, BUB1, CDCA8, TOP2A, and CCNB2)

and low TSPAN6 expression using the estimation process. The data (Fig. 6A–C) showed that the TSPAN6 high-expression group had higher stromal and immune scores, implying lower tumor purity in gliomas. Next, we compared the profiles of immune infiltration in gliomas with different TSPAN6 expression levels using ssGSEA. The findings showed a significant increase in the proportion of aDC, eosinophils, neutrophils, macrophages, helper T cells, and Th2 cells in glioma patients with high TSPAN6 expression. Conversely, patients with high TSPAN6 expression had significantly lower levels of infiltration of CD8 T cells, DC cells, pDC cells, NK CD56bright cells, and Treg cells than patients with low TSPAN6 expression (Fig. 6D). Furthermore, we investigated the relationship between TSPAN6 expression levels and immune infiltration in gliomas. The results revealed a positive correlation between TSPAN6 expression and macrophage (Fig. 6E), Th2 (Fig. 6F), aDC (Fig. 6G), eosinophil (Fig. 6H), and neutrophil infiltration (Fig. 6I). In contrast, a negative correlation was observed between the expression levels

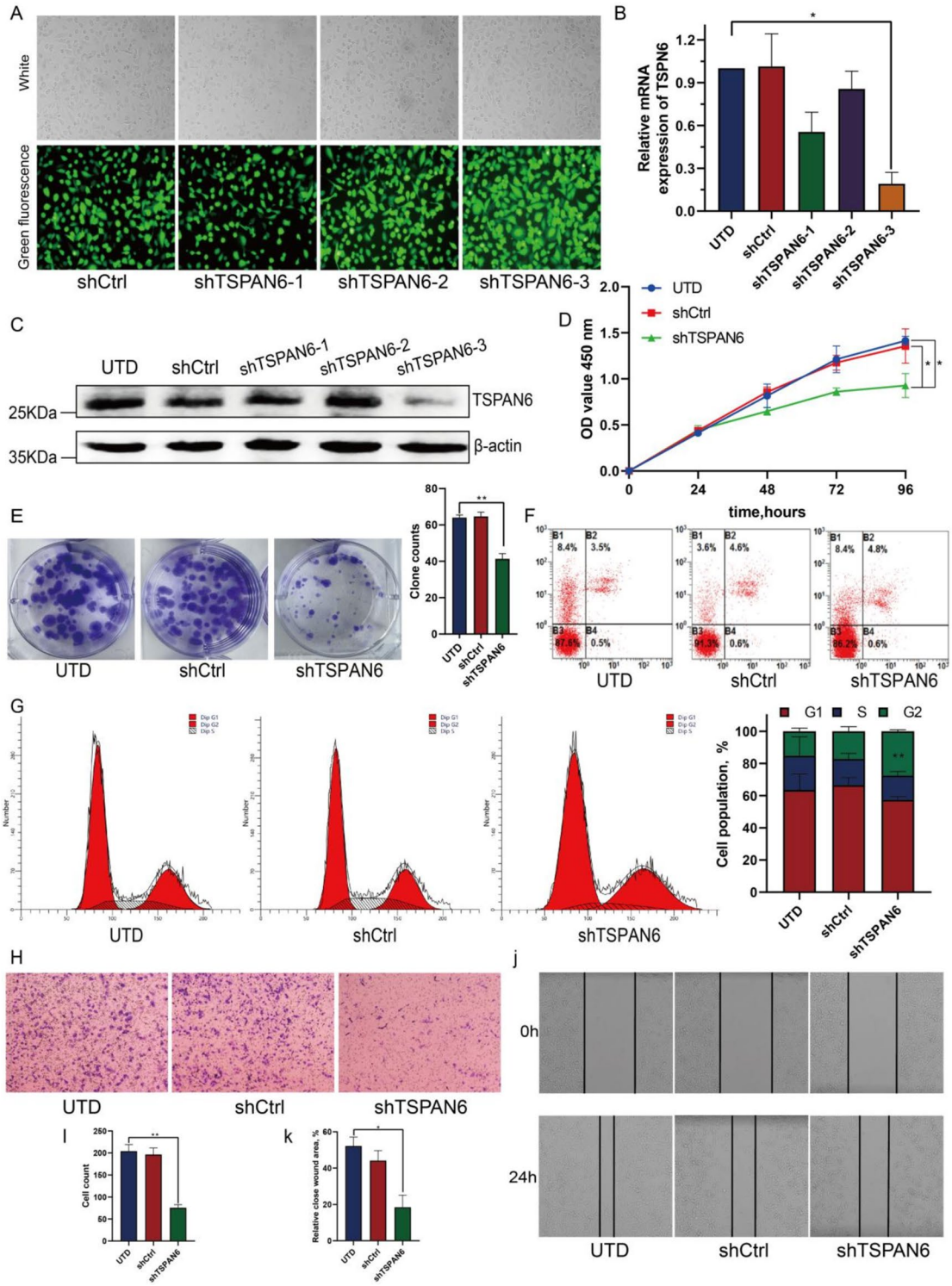

Fig. 5 Promotion of glioma cell proliferation and migration by TSPAN6. **A** Fluorescent display of lentivirus infection efficiency. **B** Changes in mRNA levels of TSPAN6 in U251 cells measured by RT-qPCR. **C** Interference efficiency of shTSPAN6 on U51 cells detected by Western blot. **D** Proliferation ability of U251 cells determined by CCK-8 assay. **E** Proliferation and colony formation ability of U251 cells measured by plate colony formation experiment. **F** Apoptosis ratio of U251 cells detected by flow cytometry. **G** Cell cycle distribution of U251 cells measured by flow cytometry. **H**, **I** Transwell experiment to measure the migration ability of U251 cells. **J**, **K** Wound healing assay to measure the migration ability of U251 cells

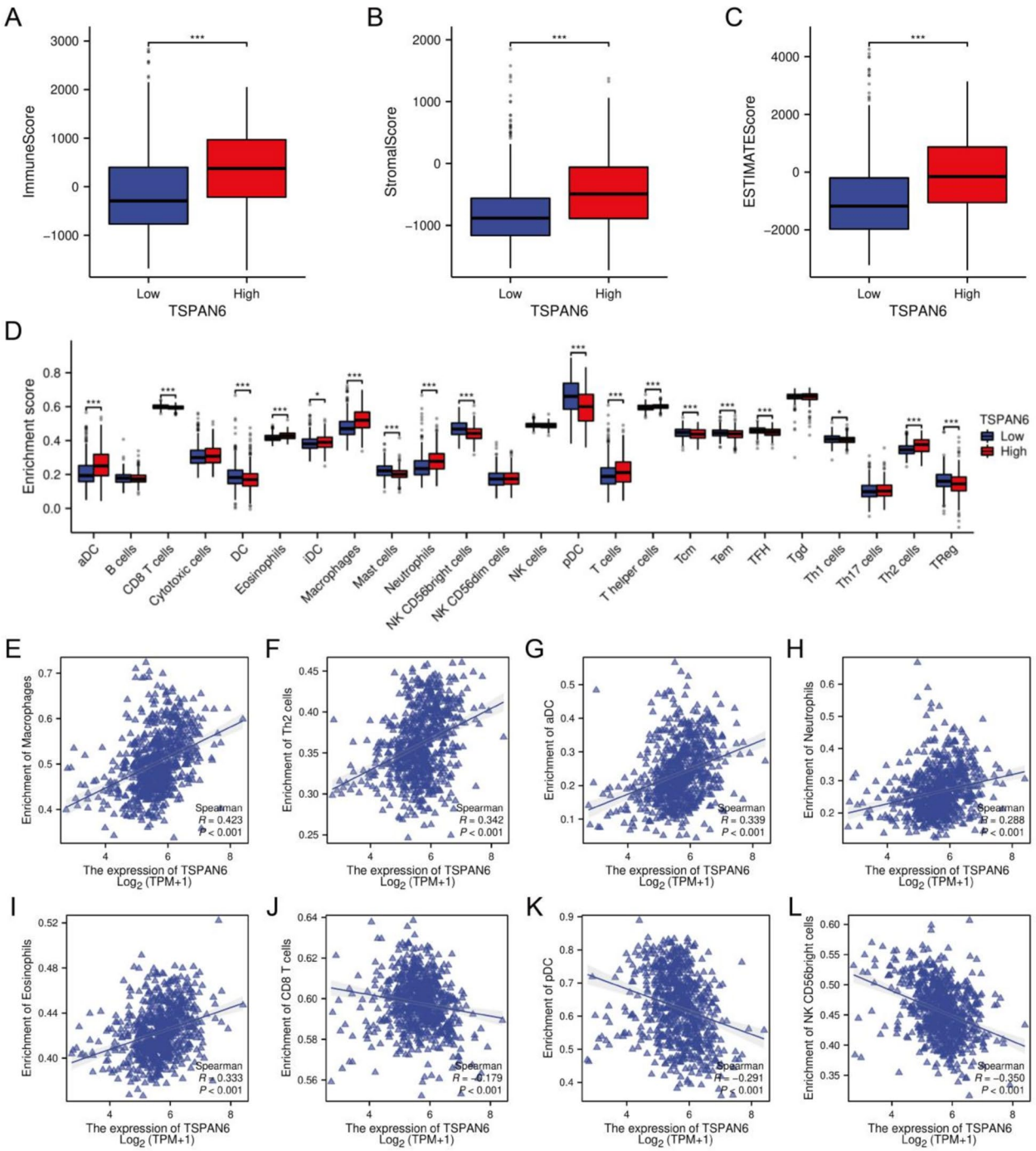

Fig. 6 **A** Immune score, **B** stromal score, and **C** estimate score between TSPAN6 high and low-expression groups in glioma. **D** Differential distribution of immune cells in TSPAN6 high and low-expression patients. The expression level of TSPAN6 positively correlates with infiltration levels of macrophages (**E**), Th2 cells (**F**), activated dendritic cells (aDC) (**G**), neutrophils (**H**), and Eosinophils (**I**), and negatively correlates with infiltration levels of CD8 T cells (**J**), plasmacytoid dendritic cells (pDC) (**K**), and NK CD56bright cells (**L**)

of TSPAN6 and CD8 T cells (Fig. 6J), pDC (Fig. 6K), and NK CD56bright cells (Fig. 6L).

Subsequently, the impact of TSPAN6 expression and M2 macrophages on the prognosis of patients with glioma was assessed using TIMER. The findings revealed that patients with high TSPAN6 expression and high levels of M2 macrophages had the poorest prognosis (Fig. 7A). To investigate the chemotactic capacity of

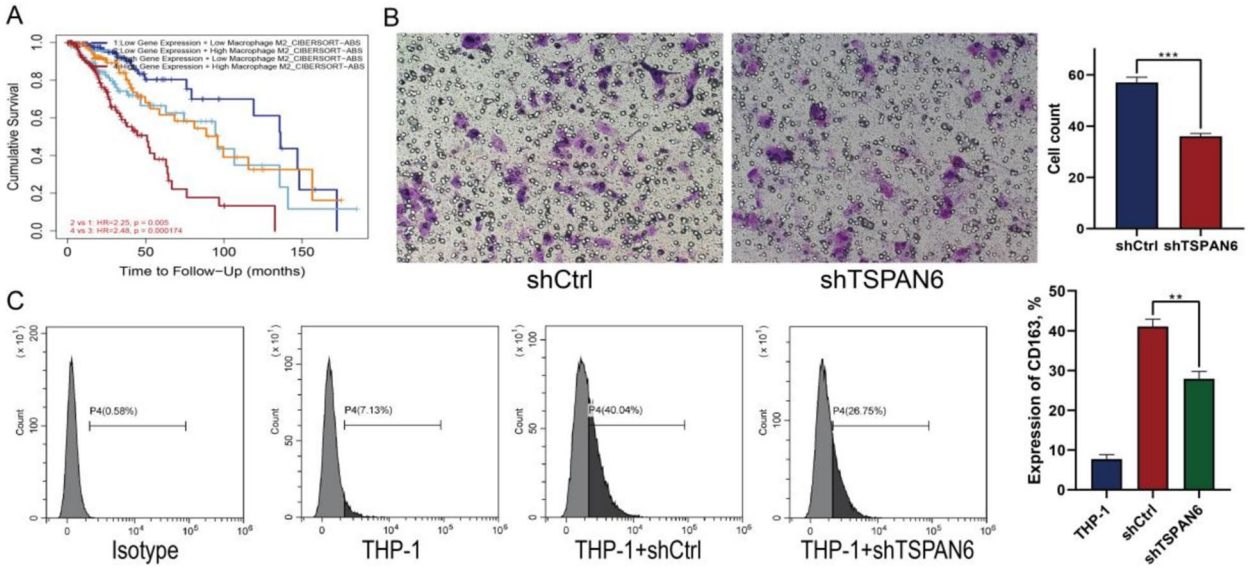

Fig. 7 Enhanced recruitment of macrophages by TSPAN6 in glioma cells. **A** Clinical survival outcome of glioma patients in the high-macrophage group. **B** Transwell experiment to measure the recruitment ability of U251 cells to macrophages. **C** Flow cytometry analysis of the effect of U251 cells on macrophage differentiation. **D** Transwell experiment to measure the invasion ability of U251 cells. **E** Wound healing assay to measure the migration ability of U251 cells

the glioma cell line towards macrophages, phorbol ester (PMA)-induced THP-1 cells were introduced into the transwell chamber, and the glioma cell line was placed in the lower chamber. Macrophages on the lower surface of the chamber were counted 48 h after the co-culture. The results showed that TSPAN6 knockdown significantly reduced macrophage recruitment by U251 cells (Fig. 7B). Finally, PMA-induced macrophages derived from THP-1 cells were co-cultured with U251 cells for 24 h. Flow cytometry was used to measure the expression of the M2-polarized marker CD163. The results indicated that TSPAN6 knockdown significantly inhibited CD163 expression (Fig. 7C), suggesting that high expression of TSPAN6 in gliomas can drive the differentiation of macrophages into immunosuppressive M2-like macrophages, potentially promoting glioma progression.

TSPAN6 is co-expressed with immune checkpoint molecules and may predict the efficacy of ICB in gliomas

We compared the expression levels of eight immune checkpoint genes (PDCD1, SIGLEC15, CD274, HAVCR2, PDCD1LG2, LAG3, CTLA4, and TIGIT) between the TSPAN6 high and the TSPAN6 low-expression groups. We found significant overexpression of all eight genes in the TSPAN6 high-expression group ($p < 0.001$) (Fig. 8A). Next, the relationship between TSPAN6 and the eight immune checkpoint genes in gliomas was assessed using Spearman's correlation analysis. The findings showed a positive correlation between TSPAN6 expression and CD274 ($p < 0.001$, $R = 0.426$; Fig. 8B), PDCD1LG2 ($p < 0.001$, $R = 0.562$; Fig. 8C), HAVCR2 ($p < 0.001$, $R = 0.417$; Fig. 8D), and PDCD1 ($p < 0.001$, $R = 0.313$; Fig. 8E). However, the correlation between TSPAN6 and CTLA4 ($p < 0.001$, $R = 0.241$; Fig. 8F), SIGLEC15 ($p < 0.001$, $R = 0.210$; Fig. 8G), TIGIT ($p < 0.001$, $R = 0.147$; Fig. 8H), and LAG3 ($p < 0.001$, $R = 0.129$; Fig. 8I) was relatively weaker.

In addition, we observed the intensity of the immune checkpoint blocking response in the low- and high-expression groups of TSPAN6. The findings revealed that the TSPAN6 high-expression group had higher TIDE scores than the TSPAN6 low-expression group in glioma patients (LGG+GBM) ($p < 0.001$, Fig. 8J), as well as in LGG ($p < 0.001$, Fig. 8K) and GBM ($p < 0.05$, Fig. 8L). In the IMvigor210 bladder cancer cohort, the ICB responsive group exhibited higher TSPAN6 expression than the ICB non-responsive group ($p < 0.001$, Fig. 8M). Subsequently, we observed the response rate to PD-L1 treatment and found that it was 23.2% in the TSPAN6 low-expression group and 35.1% in the TSPAN6 high-expression group ($p < 0.001$, Fig. 8N). Additionally, the TSPAN6 high-expression group showed a higher survival rate than the TSPAN6 low-expression group ($p = 0.0029$, Fig. 8O). These findings suggest that TSPAN6 has prognostic value for response

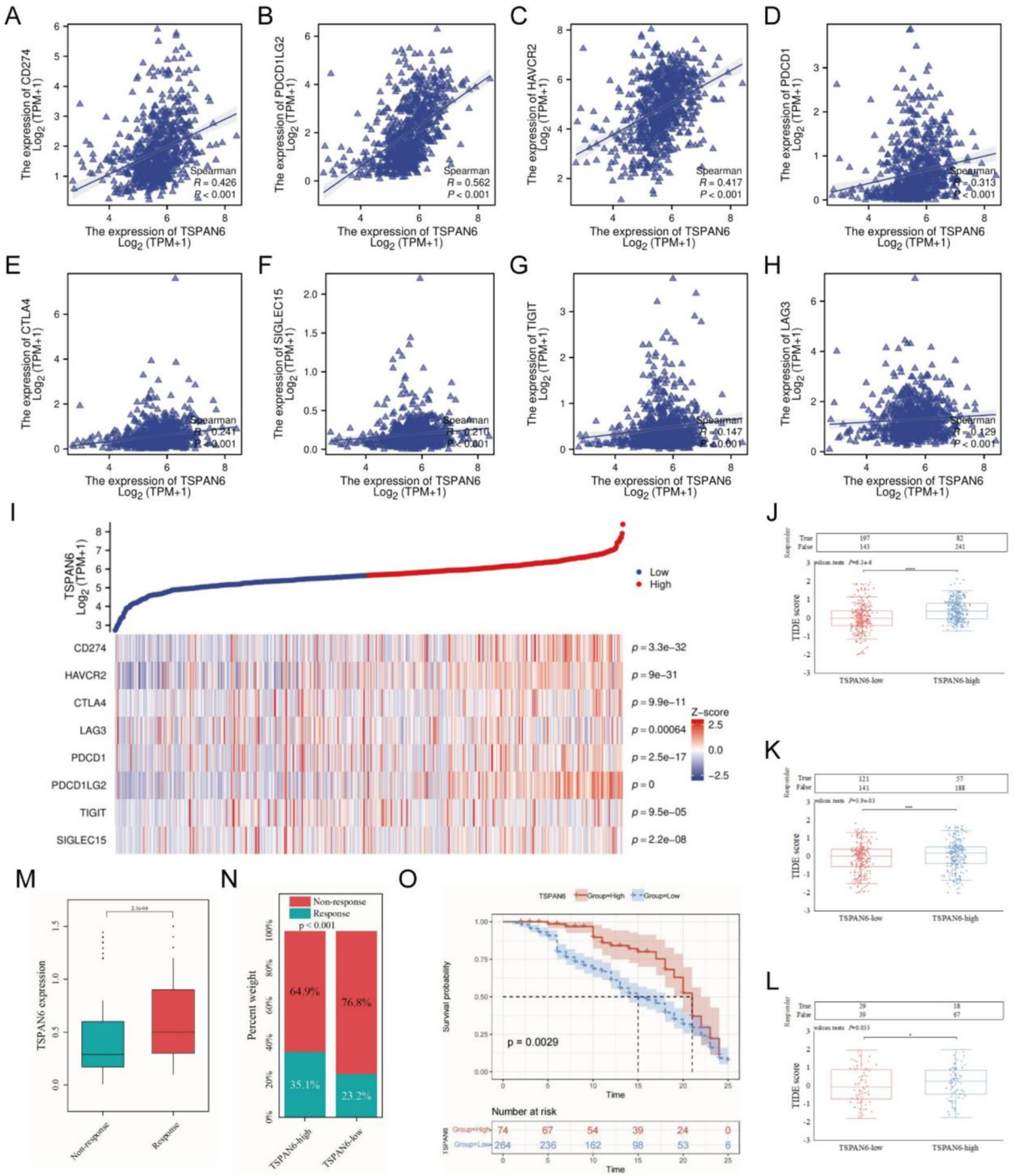

Fig. 8 Correlation of TSPAN6 with immune checkpoint genes and prediction of immune therapy response. The correlation of TSPAN6 with immune checkpoint genes CD274 (**A**), PDCD1LG2 (**B**), HAVCR2 (**C**), PDCD1 (**D**), CTLA4 (**E**), SIGLEC15 (**F**), TIGIT (**G**), and LAG3 (**H**) in glioma. **I** Heatmap of immune checkpoint gene expression in TSPAN6 high and low-expression groups. TIDE score between TSPAN6 high and low-expression groups in glioma (LGG+GBM) (**J**), LGG (**K**), and GBM (**L**). **M** Expression of TSPAN6 in responders and non-responders to anti-PD-L1 treatment in the IMvigor210 cohorts (anti-PD-L1, urothelial carcinoma). **N** Proportions of responders and non-responders in the TSPAN6 high and low-expression groups in the IMvigor210 cohorts receiving anti-PD-L1 treatment. **O** Kaplan–Meier curves of TSPAN6 high and low-expression groups in the IMvigor210 cohorts receiving anti-PD-L1 treatment

to ICB treatment, and high expression of TSPAN6 may be more favorable for ICB therapy.

Discussion

Glioma, with its high incidence and recurrence rate, is among the most prevalent primary malignant tumors of the brain and spinal cord. Despite undergoing surgical treatment, patients often have a poor prognosis due to the tumor's specific location. Therefore, there is an urgent need to identify biomarkers that can assist in diagnosis, prognosis, and treatment decisions. The TSPAN family currently includes 33 subtypes identified in both humans and mice [4]. The specific roles and functions of these subtypes are not well understood because of their large numbers, and some subtypes are still in the speculative stage. For instance, in cholangiocarcinoma, the growth and migration of cholangiocarcinoma cells are regulated by the interaction between TSPAN1 and integrin α6β1, accomplished through upregulation of the PI3K/AKT/GSK-3β/Snail/PTEN feedback loop [26]. Similarly, in colorectal cancer, high expression of TSPAN12 is significantly correlated with TNM stage, tumor size, and lymph node metastasis. Knockdown of TSPAN12 significantly reduces the growth, migration, and invasion abilities of colorectal cancer cells and promotes apoptosis [27]. Furthermore, TSPAN6 expression can inhibit tumor tissue growth and metastasis in mutant pancreatic cancer xenografts, which is influenced by RAS activation [9]. However, there are currently no reports on the involvement of TSPAN6 in gliomas.

This study aimed to investigate the biological roles and potential regulatory mechanisms of TSPAN6 in gliomas through comprehensive bioinformatics analysis using multiple publicly available datasets. The findings of this study showed an upregulation of TSPAN6 expression across multiple tumor types, including gliomas. The overexpression of TSPAN6 was correlated with decreased survival rates and unfavorable clinicopathological characteristics. ROC curve analysis suggested that TSPAN6 might be a promising biomarker for glioma diagnosis. There was a strong correlation between TSPAN6 expression and glioma prognosis, indicating an independent effect of TSPAN6 on glioma prognosis. Accordingly, we investigated the mechanism underlying reduced survival rates in patients with glioma associated with TSPAN6. GSEA provided additional confirmation of this result. GO and KEGG analyses indicated that DEGs related to TSPAN6 were primarily associated with tumor cell division and cell cycle regulation. Additionally, we identified 10 significant DEGs (CCNA2, CCNB1, CDC20, BUB1, CCNB2, TOP2A, CDCA8, NDC80, RRM2, and DLGAP5). Interestingly, the results of the GO and KEGG analyses also demonstrated a connection between cell cycle signaling and the obtained outcomes. Prior research has demonstrated that cancer and normal cells express unique cell cycle protein genes [27]. Our results suggest a positive correlation between the expression of TSPAN6 and cell cycle regulatory genes. Additionally, cell cycle experiments have demonstrated that TSPAN6 knockdown induces G2/M phase cell cycle arrest in glioma cells. Furthermore, colony formation and CCK-8 assays confirmed the inhibitory effect of TSPAN6 suppression on glioma cell proliferation. In conclusion, our findings suggest that TSPAN6 plays a regulatory role in the cell cycle and promotes glioma growth.

The incidence of malignant tumors is closely associated with the TME, which comprises immune cells, stromal cells, extracellular matrix, and inflammatory mediators. Dysregulation of the immune response within the TME is a leading factor in glioblastoma development. This study examined the relationship between TSPAN6 expression and extent of immune infiltration in glioblastoma. These findings indicated a positive correlation between high TSPAN6 expression and the extent of macrophage infiltration. Growing evidence suggests that macrophages in glioblastoma promote tumor growth and invasion by modulating immune surveillance and suppressing antitumor immune responses, thereby playing a detrimental role in cancer progression [28]. TSPAN6 could chemotactically attract macrophages to migrate towards tumor cells and differentiate into immunosuppressive M2 macrophages. These findings suggest that TSPAN6 may contribute to glioblastoma development by influencing macrophages in the TME.

Recently, ICB has been proven to extend the survival of many patients with cancer and provide new ideas and options for personalized treatment [29]. Tumor cells employ multiple mechanisms to evade the immune system, with one of them being the continuous amplification of immune suppression signals. Most tumor cells upregulate the immune checkpoint ligand PD-L1, which inhibits the function of lymphocytes by binding to PD-1 receptors on tumor-infiltrating lymphocytes (TILs), enabling tumor immune escape [30, 31]. In addition to the conventional immune checkpoints PD-1/PD-L1, CTLA4, and LAG3, studies have shown that blocking additional immune regulatory genes, such as LGALS1 [32] and IGFBP2 [33], also improves the suppressive TME of glioblastoma. Recent advancements in the application of ICB in glioblastoma, although benefiting only a subset of patients, point towards using biomarkers to guide immunotherapy and develop personalized treatments [34]. Our research findings indicate a correlation between the expression of TSPAN6 and a subset of immune checkpoints in patients with glioblastoma. The high TSPAN6 expression group exhibited higher gene expression levels

for specific immunological checkpoints compared to the low TSPAN6 expression group. Additionally, TIDE scoring was used to assess the relationship between TSPAN6 expression and the strength of the ICB response. The findings revealed that the group with higher TSPAN6 expression had higher TIDE scores. These results suggest that in glioblastoma, TSPAN6 expression is associated with a subset of immune checkpoints, and glioblastoma patients with high TSPAN6 expression may benefit from ICB treatment. Therefore, we propose that TSPAN6 could potentially be a predictive biomarker for the intensity of the ICB response in glioblastoma patients.

Despite our comprehensive analysis of TSPAN6, our study has several notable limitations. Firstly, our conclusions are predominantly derived from public database data, underscoring the need for additional in vitro and in vivo experiments to validate our findings and elucidate the exact mechanisms underlying TSPAN6's role. Secondly, although our study shows a strong correlation between TSPAN6 expression and immune infiltration, it remains unconfirmed whether TSPAN6 can promote the infiltration of tumor-associated macrophages in glioma samples. Further research is also required to clarify its impact on cytokine expression within the glioma tumor microenvironment.

Conclusion

In conclusion, our research demonstrates a significant upregulation of TSPAN6 expression in gliomas, which is strongly associated with the pathological and clinical characteristics, as well as the unfavorable prognosis of gliomas. According to ROC analysis, TSPAN6 can be used as a prognostic biomarker for glioma patients and as a diagnostic biomarker to differentiate glioma tissue from normal tissue. By regulating the process of immune infiltration, TSPAN6 may contribute to the development of glioma and may serve as a predictive biomarker for the degree of ICB response in glioma patients.

Abbreviations

TSPAN	Tetraspanin
TCGA	The Cancer Genome Atlas
GEO	Gene Expression Omnibus
GO	Gene Ontology
KEGG	Kyoto Encyclopedia of Genes and Genomes
GSEA	Gene Set Enrichment Analysis
OS	Overall survival
PFI	Progression free interval
DSS	Disease specific survival
GTEx	Genotype-tissue expression
ROC	Receiver operating characteristic
AUC	A closer region under the curve
NES	Normalized enrichment score
GBM	Glioblastoma
LGG	Low-grade glioma
CI	Confidence interval
DEGs	Differentially expressed genes
FDS	False discovery rate
FBS	Fetal bovine serum
ICB	Immune checkpoint blockade
TME	Tumor microenvironment
TAMs	Tumor-associated macrophages
PPI	Protein–protein interaction
ssGSEA	Single-sample Gene Set Enrichment Analysis
TIDE	Tumor immune dysfunction and exclusion
GFP	Green fluorescent protein

Supplementary Information

The online version contains supplementary material available at https://doi.org/10.1186/s40001-024-02119-5.

Supplementary Material 1.

Acknowledgements

We acknowledge the Medical Innovation Center of the Fourth Military Medical University for providing the equipment and service support.

Author contributions

Conceptualization, T.W. and L.S.; methodology, L.S., Y.H. and L.L.; validation, H.Z., L.Z. and W.Z.; formal analysis, L.S.; investigation, T.W and L.S.; data curation, L.S., H.Z. and Y.H.; writing—original draft preparation, L.S.; writing—review and editing, T.W.; supervision, T.W and L.S.; project administration, T.W and L.S.; funding acquisition, T.W. and L.S.

Funding

This research was funded by grants from the National Natural Science Foundation of China, Grant Number 82073361; the State Key Laboratory of Cancer Biology Project, grant number CBSKL2022ZZ21; the Key R&D Plan of Shaanxi Province, grant number 2023-YBSF-667; the Xi'an Municipal Health Commission grant, Grant Number 2022ms06.

Availability of data and materials

No datasets were generated or analysed during the current study.

Declarations

Ethics approval and consent to participate

All methods were carried out in accordance with the Declaration of Helsinki. No ethics approval was required for this work. All utilized public data sets were generated by others who obtained ethical approval.

Consent for publication

Not applicable.

Competing interests

The authors declare no competing interests.

Author details

[1]Department of Spine Surgery, Honghui Hospital, Xi'an Jiaotong University, Xi'an 710054, China. [2]State Key Laboratory of Holistic Integrative Management of Gastrointestinal Cancers, Department of Medical Genetics and Developmental Biology, Fourth Military Medical University, Xi'an 710032, China. [3]The Fifth Cadet Regiment, Fourth Military Medical University, Xi'an 710032, China.

Received: 6 February 2024 Accepted: 17 October 2024
Published online: 29 October 2024

References

1. Global Burden of Disease Cancer Collaboration, et al. Cancer incidence, mortality, years of life lost, years lived with disability, and disability-adjusted life years for 29 cancer groups from 2010 to 2019: a systematic

analysis for the global burden of disease study 2019. JAMA Oncol. 2022;8(3):420–44.
2. Louis DN, et al. The 2016 World Health Organization classification of tumors of the central nervous system: a summary. Acta Neuropathol. 2016;131(6):803–20.
3. Louis DN, et al. The 2021 WHO classification of tumors of the central nervous system: a summary. Neuro Oncol. 2021;23(8):1231–51.
4. Charrin S, et al. Tetraspanins at a glance. J Cell Sci. 2014;127(Pt 17):3641–8.
5. Florin L, Lang T. Tetraspanin assemblies in virus infection. Front Immunol. 2018;9:1140.
6. Cai Y, et al. Expression of Tspan-1 gene in patients with advanced gastric cancer. Oncol Lett. 2017;14(3):2996–3000.
7. Zhang X, et al. TSPAN1 upregulates MMP2 to promote pancreatic cancer cell migration and invasion via PLCgamma. Oncol Rep. 2019;41(4):2117–25.
8. Lu X, et al. EGFR signaling promotes nuclear translocation of plasma membrane protein TSPAN8 to enhance tumor progression via STAT3-mediated transcription. Cell Res. 2022;32(4):359–74.
9. Humbert PO, et al. TSPAN6 is a suppressor of Ras-driven cancer. Oncogene. 2022;41(14):2095–105.
10. Andrijes R, et al. Tetraspanin 6 is a regulator of carcinogenesis in colorectal cancer. Proc Natl Acad Sci USA. 2021;118(39): e2011411118.
11. Xu-Monette ZY, et al. Assessment of CD37 B-cell antigen and cell of origin significantly improves risk prediction in diffuse large B-cell lymphoma. Blood. 2016;128(26):3083–100.
12. Komohara Y, et al. Possible involvement of the M2 anti-inflammatory macrophage phenotype in growth of human gliomas. J Pathol. 2008;216(1):15–24.
13. Massara M, et al. Neutrophils in gliomas. Front Immunol. 2017;8:1349.
14. Rahbar A, et al. Enhanced neutrophil activity is associated with shorter time to tumor progression in glioblastoma patients. Oncoimmunology. 2016;5(2): e1075693.
15. Schadendorf D, et al. Pooled analysis of long-term survival data from phase II and phase III trials of ipilimumab in unresectable or metastatic melanoma. J Clin Oncol. 2015;33(17):1889–94.
16. Brahmer JR, et al. Phase I study of single-agent anti-programmed death-1 (MDX-1106) in refractory solid tumors: safety, clinical activity, pharmacodynamics, and immunologic correlates. J Clin Oncol. 2010;28(19):3167–75.
17. Wang C, Yu M, Zhang W. Neoantigen discovery and applications in glioblastoma: an immunotherapy perspective. Cancer Lett. 2022;550: 215945.
18. Cerami E, et al. The cBio cancer genomics portal: an open platform for exploring multidimensional cancer genomics data. Cancer Discov. 2012;2(5):401–4.
19. Gao J, et al. Integrative analysis of complex cancer genomics and clinical profiles using the cBioPortal. Sci Signal. 2013;6(269): pl1.
20. Forbes SA, et al. COSMIC (the catalogue of somatic mutations in cancer): a resource to investigate acquired mutations in human cancer. Nucleic Acids Res. 2010;38(1):D652–7.
21. Yu G, et al. clusterProfiler: an R package for comparing biological themes among gene clusters. OMICS. 2012;16(5):284–7.
22. Bindea G, et al. Spatiotemporal dynamics of intratumoral immune cells reveal the immune landscape in human cancer. Immunity. 2013;39(4):782–95.
23. Hu X, et al. The oncogenic role of tubulin alpha-1c chain in human tumours. BMC Cancer. 2022;22(1):498.
24. Hu X, et al. Tubulin alpha 1b is associated with the immune cell infiltration and the response of HCC patients to immunotherapy. Diagnostics. 2022;12(4):858.
25. Tu Z, et al. Protein disulfide-isomerase A3 is a robust prognostic biomarker for cancers and predicts the immunotherapy response effectively. Front Immunol. 2022;13: 837512.
26. Wang Y, et al. Tetraspanin 1 promotes epithelial-to-mesenchymal transition and metastasis of cholangiocarcinoma via PI3K/AKT signaling. J Exp Clin Cancer Res. 2018;37(1):300.
27. Liu J, et al. Upregulation of TSPAN12 is associated with the colorectal cancer growth and metastasis. Am J Transl Res. 2017;9(2):812–22.
28. Hambardzumyan D, Gutmann DH, Kettenmann H. The role of microglia and macrophages in glioma maintenance and progression. Nat Neurosci. 2016;19(1):20–7.
29. Pointer KB, Pitroda SP, Weichselbaum RR. Radiotherapy and immunotherapy: open questions and future strategies. Trends Cancer. 2022;8(1):9–20.
30. Gordon SR, et al. PD-1 expression by tumour-associated macrophages inhibits phagocytosis and tumour immunity. Nature. 2017;545(7655):495–9.
31. Boussiotis VA. Molecular and biochemical aspects of the PD-1 checkpoint pathway. N Engl J Med. 2016;375(18):1767–78.
32. Chen Q, et al. Immunogenomic analysis reveals LGALS1 contributes to the immune heterogeneity and immunosuppression in glioma. Int J Cancer. 2019;145(2):517–30.
33. Cai J, et al. Immune heterogeneity and clinicopathologic characterization of IGFBP2 in 2447 glioma samples. Oncoimmunology. 2018;7(5): e1426516.
34. Arrieta VA, et al. Immune checkpoint blockade in glioblastoma: from tumor heterogeneity to personalized treatment. J Clin Invest. 2023;133(2): e163447.

Publisher's Note